Destination Mars: Frontiers in Expanding Human Presence in the Solar System

Ahsan Choudhuri, Ph.D.
Professor and Chair, Department of Mechanical Engineering
Mr. and Mrs. MacIntosh Murchison Chair II in Engineering
Director, NASA URC: Center for Space Exploration Technology Research
University of Texas at El Paso
E-mail: ahsan@utep.edu

This presentation provides an overview of the rationale and key technical challenges of the human exploration of Mars. Although the compulsion to explore Mars originates from the desire of human beings to explore, several key scientific questions provide the necessary underpinning for the Marsto be the next destination of human exploration. As a part of the inner planets of the solar system Mars has similar features such as atmosphere, polar ice cap, four seasons, and climate cycle like the planet Earth. The past and present orbiter and lander missions have revealed many interesting Earth like geological features (mountains, canyons, plateaus, and in-active volcanos) and confirmed the presence of water in the Martian atmosphere, in the subsurface, and soil. Scientific data collected through these missions indicate that Mars might have been warmer and wetter in the past. Although the surface conditions of the present-day Mars are inhospitable to terrestrial life, there is sufficient scientific evidence that around 3.5 billion years ago Mars may have had an environment conducive to the formation of lifefor over several hundred million years. Human exploration of Mars thus provides a compelling choice for understanding the origin of life on Earth, searching for life in the solar system, and developing a permanent human settlement.

From the first successful Mars fly-by mission of Mariner 4 spacecraft in 1964 to the most recent Mars Science Laboratory Rover*Curiosity* in 2012, the United States has been in the forefront of exploring the planet Mars through orbiter and robotic lander missions. The data collected from these missions have significantly improved the understanding of the geology and atmosphere of the Mars as well as advancing spacecraft technologies needed for the human spaceflight.The human spaceflight to Mars requires many technological advances as well significant budgetary and policy supportto develop complex space transportation, life-support, radiation shielding, and surface operation systems.NASA's exploration systems development effort which include the Orion Crew Exploration Vehicle (Orion CEV), Space Launch System (SLS), and Ground Systems will enable human exploration to deep space destinations including Mars.

The Center for Space Exploration Technology Research (cSETR) at the University of Texas at El Paso is a NASA University Research Center focusing on developing LO_2/LCH_4 propulsion technologies to support NASA's Mars Exploration strategies. The integrated LO_2/LCH_4 human spaceflight spacecraft architecture is based on utilizing a common fluid system (LO_2-LCH_4 for propulsion, power, and environmental control and life-support systems) scavenged from Martian atmosphere and surface using In-Situ Resource Utilization (ISRU) techniques. The LO_2/LCH_4 architecture has the potential to reduce 280 metric tons of initial launch masses to Low Earth Orbit (IMLEO) if 25 metric tons of oxygen can be produced in Mars for the Mars Ascent Vehicle (MAV). Additional IMLEO savings can also be achieved through possible production of methane using the water on Mars.

About the Speaker:Dr. Ahsan Choudhuri is a Professor and Chair of Mechanical Engineering and director and founder of the NASA funded Center for Space Exploration Technology Research at the University of Texas at El Paso, where he also holds the endowed Mr. and Mrs. MacIntosh Murchison Chair II in Engineering. Dr. Choudhuri received degrees in mechanical engineering from Khulna University of Engineering and Technology (B.S., 1992) and the University of Oklahoma (M.S., 1997, and Ph.D., 2000). Professor Choudhuri's teaching and research interests are in the area of aerospace systems and energy engineering. Dr. Choudhuri's current and previous research efforts include non-toxic cryogenic propulsion systems (NASA), fuel flexible gas turbine combustors (Department of Energy), oxy-fuel combustors (Department of Energy), materials for advanced turbines (Department of Energy), next generation green and solid propellants (Missile Defense Agency), turbopump technology for advanced liquid propellant rocket engines (Missile Defense Agency, NASA), advanced divert and attitude control systems for missile interceptors (Space and Missile defense command and Missile Defense Agency), and microgravity combustion and materials science (NASA).

AboutThe Center for Space Exploration Technology Research (cSETR):The Center for Space Exploration Technology Research (cSETR) at the University of Texas El Paso supports NASA's vision of space exploration by focusing on advanced capabilities in the areas of non-toxic and green propulsion. The cSETR vision is to establish a sustainable minority university center of excellence in advanced propulsion research through strategic partnerships and to educate a diverse future aerospace workforce. To achieve this vision and create advanced technologies and exploration capabilities for lunar, mars, solar system and beyond missions, a multidisciplinary engineering team partners with NASA centers (Johnson Space Center-lead NASA partner, Marshall Space Flight Center, Glenn Research Center, and NASA White Sands Test Facility), aerospace industries (Lockheed Martin Inc., Blue Origin, and ATK), and academic institutions (University of Maryland and Princeton University).

ICMIEE-PI-Keynote

Flow-Induced Forces and Fluid-Structure Interactions between Two Circular Cylinders

Md. Mahbub Alam [a,b,*]

[a]Institute for Turbulence-Noise-Vibration Interaction and Control, Shenzhen Graduate School
Harbin Institute of Technology, Shenzhen, China
[b]Key Kab of Advanced Manufacturing and Technology, Shenzhen Graduate School
Harbin Institute of Technology, Shenzhen, China

ABSTRACT
Flow-induced fluctuating lift (C_{Lf}) and drag (C_{Df}) forces and Strouhal numbers (St) of the downstream cylinder of two tandem cylinders are investigated experimentally for Reynolds number (Re) = 9.7×10^3 ~ 6.5×10^4. The spacing ratio L^* (= L/D) between the cylinders is varied from 1.1 to 4.5, where L is the spacing between the cylinders and D is the cylinder diameter. The results show that C_{Lf}, C_{Df} and St are highly sensitive to Re due to change in the inherent nature of the flow structure. How the flow structure is dependent on Re and L^* is presented in a flow structure map. Zdravkovich and Pridden in 1977 observed a 'kink' in time-mean drag distribution at $L^* \approx 2.5$ for Re > 3.1×10^4, but not for Re ≤ 3.1×10^4. The physics is provided here behind the presence and absence of the 'kink' that was left unexplained since then.

Keywords: fluid forces; tandem cylinders; fluid-structure interaction, flow structures, Strouhal numbers

1. Introduction

The flow over a circular cylinder is a classical case, studied extensively for over 100 years, as it contains a wide range of complex flow phenomena, despite its simple geometry. The flow displays different characteristics at different Re regimes. The most famous is the formation of the von Kármán vortex street, where counter-rotating vortices are shed from the cylinder in a periodic fashion [1]. This class of flow evolves in complexity when an additional cylinder is placed in the wake of the other [2].

Slender structures appear in groups in many engineering applications, for example, chimney stacks, tube bundles in heat exchangers, cooling of electronic equipments, high-rise buildings, overhead power-line bundles, bridge piers, stays, and chemical-reaction towers. Naturally, some structures in a group are submerged in the wake of the others. Two inline cylinders may be considered as the basic element of multiple structures, where the leeward cylinder is in the wake of the windward cylinder (Fig. 1a). The knowledge of this flow is insightful for understanding the flow around structures in groups.

The in-line configuration of two cylinders involves shear-layer and cylinder interaction that is strongly dependent on Re and L^*. The characteristics of the flow

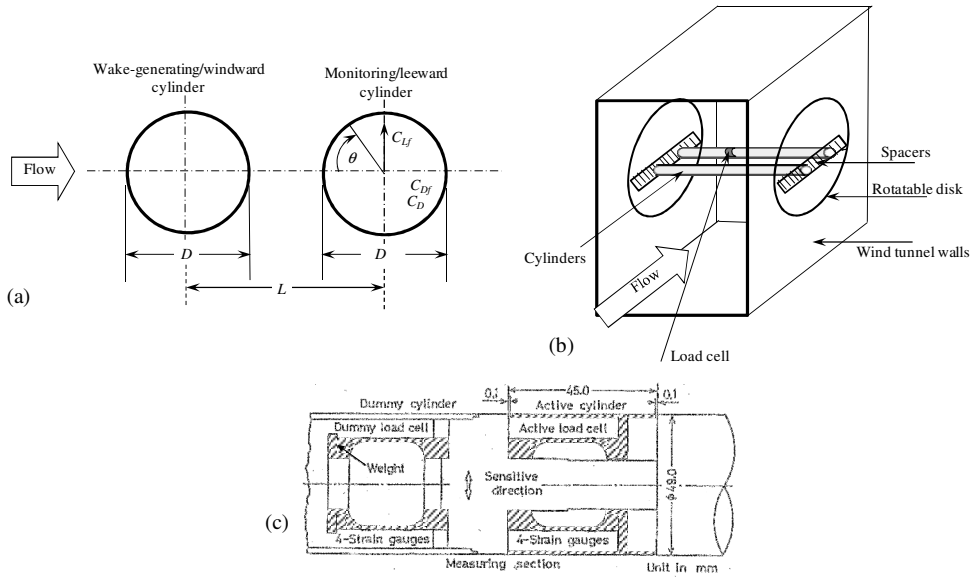

Fig. 1 (a) Notation of cylinder configuration, (b) a schematic of experimental setup, and (c) load cell details.

* Corresponding author. Tel.: +86-15014047005
E-mail address: alamm28@yahoo.com; alam@hitsz.edu.cn

around two cylinders has been extensively reviewed by [3].

Biermann and Herrnstein [4] measured time-averaged drag (C_D) on the two inline cylinders up to $L^* = 8$ (Re = 1.05×10^5). Therefore, more investigation was needed to clarify the other parameters, such as, C_{Df}, C_{Lf}, St, surface pressures, wakes, boundary layers, etc. Time-averaged pressure measurements were conducted by Zdravkovich and Pridden [5] at Re = 6×10^4 and Alam et al. [6] at Re = 6.5×10^4. The results showed that for $L^* <$ 3.5 a negative pressure on the front surface of the leeward cylinder was generated instead of a positive pressure, exceeding that on the rear surface. In case of the windward cylinder, the pressure only on rear surface was affected by the presence of the leeward cylinder.

Igarashi [7] examined the Re effects on St and pressure fluctuations for Re = 8.7×10^3 ~ 5.2×10^4, and noted that with increasing Re the pressure fluctuation on the cylinder surfaces increased and St decreased greatly between Re = 1×10^4 and 4×10^4. Zdravkovich and Pridden [5] examined the Re effect on C_D at Re = 3.1×10^4 ~ 1.2×10^5. When the two cylinders were in contact, C_D on the leeward cylinder was negative, increasing rapidly with L^*. An interruption of the increase rate occurred, forming a 'kink' at $L^* \approx 2.5$. The 'kink' was, however, absent at Re $\leq 3.1\times10^4$. The physics behind the presence and absence of the 'kink' was left unexplained, with a notation "further research is necessary to clarify this change at small Re". The literature focus in general on flow, C_D, and St for certain Re, barely giving any attention to C_{Df} and C_{Lf} in spite of the fact that the latter is of both fundamental and practical importance in fluid-structure interaction [8]. Measuring C_{Df}, C_{Lf} on two inline cylinders at Re = 6.5×10^4 for $L^* < 9$, Alam et al. [6] observed that C_{Df} and C_{Lf} on the rear cylinder are highly sensitive to L^*. Some other imperative questions left unexplained, such as, what are their dependences on Re? What is the physics behind the 'kink'? The objective of this work is to answer the above questions.

2. Experimental details

Experiments were conducted in a low-speed, closed-circuit wind tunnel with a test section of 1.20 m in height, 0.30 m in width, and 2.2 m in length (Fig. 1b). The diameter of each cylinder was 49 mm. Re based on cylinder diameter and free-stream velocity was 9.7×10^3, 1.6×10^4, 3.2×10^4, and 6.5×10^4. Surface oil-flow visualization was also conducted to get information on the shear layer reattachment and boundary layer separation. See Alam et al. [6] for details of the visualization. Flow-induced forces were measured over a small spanwise length of the leeward cylinder, using load cells (Fig. 1c). The cylinder was built in with an active ('live') section of a spanwise 45 mm ($0.92D$) length and two dummy sections. See Alam et al. [9] for details of the load cell. Definition of symbols and coordinate systems can be seen in Fig. 1(a). The position of a point on the surface of a cylinder is defined by the azimuthal angle θ, measured from the direction of free-stream flow. Experiments were performed for L^* = 1.1 ~ 4.5. Very fine-tuning of L^* ($\Delta L^* = 0.1, 0.2$) was adopted.

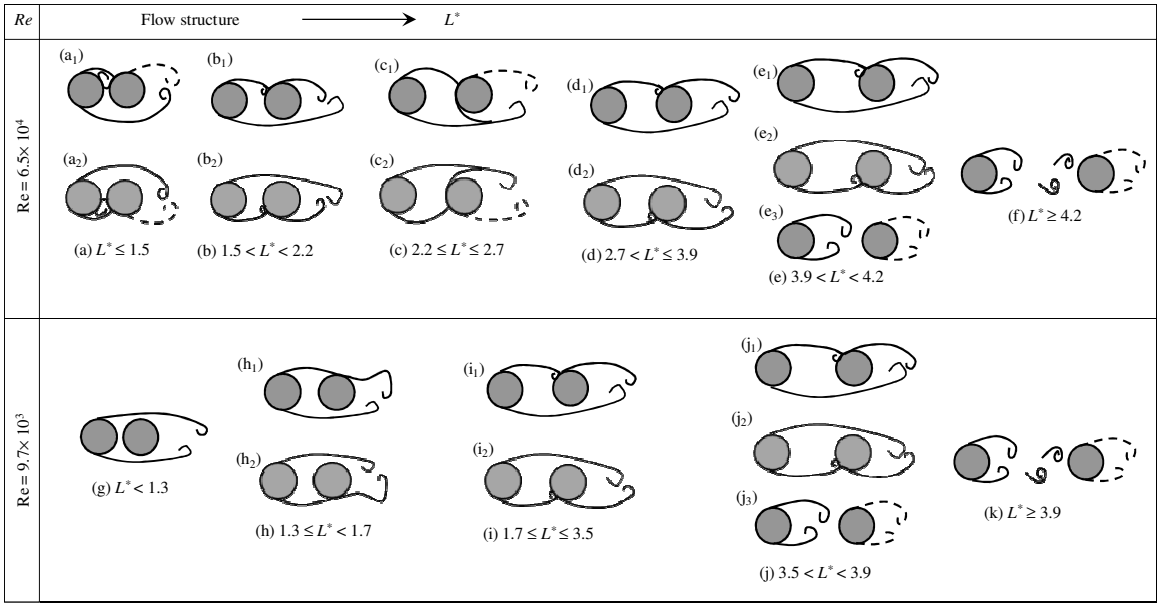

Fig. 2 Flow structures with variation in Re and L^*. (a) reverse-flow reattachment (RFR) flow, (b) front-side reattachment (FSR) flow, (c) front reattachment (FR) flow, (d) front-side reattachment (FSR) flow, (e) bi-stable (BS) flow between front-side reattachment and co-shedding flow, (f) co-shedding (CS) flow, (g) Over-shoot (OS) flow, (h) rear-side reattachment (RSR) flow, (i) front-side reattachment (FSR) flow, (j) bi-stable (BS) flow between front-side reattachment and co-shedding flows, and (k) co-shedding (CS) flow. While the solid lines represent the windward cylinder shear layers, the dashed lines stand for the leeward cylinder generated shear layers. Flow is from left to right.

3. Results and Discussion

3.1 Fluctuating forces and flow structures

Surface oil-flow visualization results are very informative, providing details of flow on the surface of the cylinder. It was found that the flow structures at Re = 6.5×10^4 and 9.7×10^3 were qualitatively similar to those at Re = 3.2×10^4 and 1.6×10^4, respectively. Therefore a sketch of flow structures based on the surface oil-flow results is presented in Fig. 2 at Re = 6.5×10^4 and 9.7×10^3 only, which will explain perspicuously the dependence of C_{Df}, C_{Lf} and St on Re and L^* in the subsequent paragraphs. Figure 3 presents C_{Df} and C_{Lf} variations with L^* and Re. C_{Df} and C_{Lf} at L^* < 3 are highly sensitive to L^* at Re = 3.2×10^4 and 6.5×10^4 but less at Re = 9.7×10^3 and 1.6×10^4. They wane with a decrease in Re, being very high at Re = 6.5×10^4.

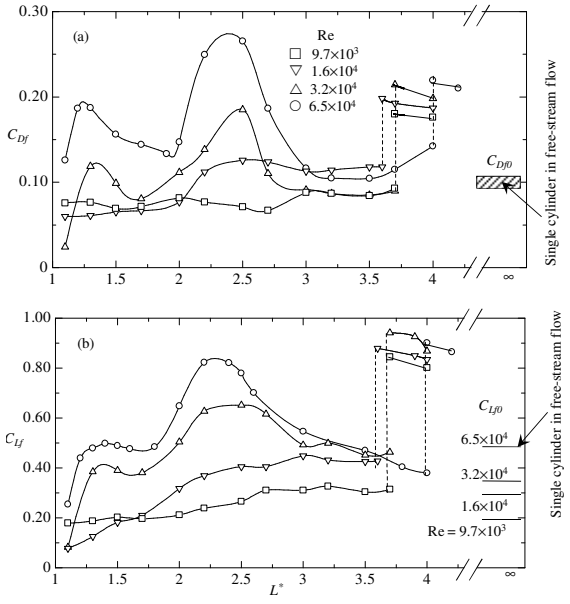

Fig. 3 Dependence of (a) C_{Df} and (b) C_{Lf} on Re and L^*.

Two peaks at L^* = 1.3 and 2.4, respectively, are formed at Re = 3.2×10^4 and 6.5×10^4 but not at Re = 9.7×10^3 and 1.6×10^4 (Fig. 3). That is, the peak at L^* = 2.4 in C_{Df} and C_{Lf} is connected to the 'kink' in C_D profile found by Zdravkovich and Pridden [5]. C_{Df} and C_{Lf} at this L^* are $2.8C_{Df0}$ and $2.0C_{Lf0}$, respectively, where the subscript '*0*' refers to a single cylinder subjected to the free-stream flow. A front-side reattachment flow is ascribed to the enhanced C_{Df} and C_{Lf} at L^* = 1.3, where the windward cylinder shear layer (solid lines) after the reattachment at θ = 66° on the leeward cylinder reverses to windward cylinder (Fig. 2a). On the other hand, at L^* = 2.4, the shear layer reattaches on the front surface at θ = 55° and goes to the other side sweeping the front surface (Fig. 2c). Here front, front-side, rear-side and rear surfaces are defined as θ = 0° ~ 60°, 60° ~ 90°, 90° ~ 120°, and 120° ~ 180°, respectively. The reattachments of the two shear layers of the windward cylinder occurred in an alternating fashion; for instance, in the first half cycle the upper shear layer (Fig 2(a_1, c_1)) reattaches and in the next half cycle the lower shear layer reattaches (Fig. $2a_2$, c_2). Beyond the critical L^* (dashed vertical lines, Fig. 3), the cylinder experiences much higher C_{Df} and C_{Lf} additionally contributed from the alternating vortices approaching from the windward cylinder (Fig. 2f, k).

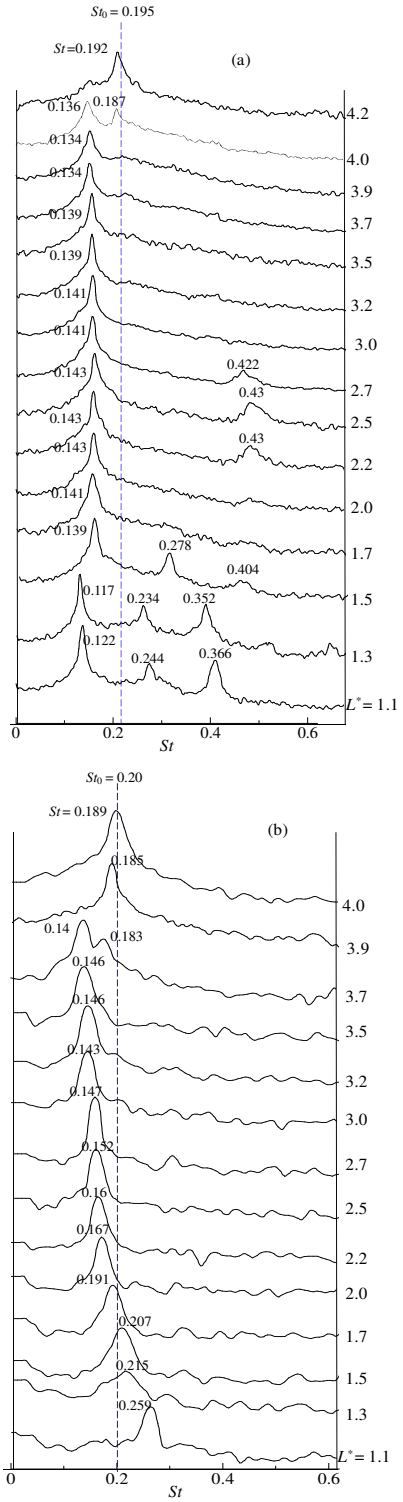

Fig. 4 Fourier power spectrum of fluctuating lift on the leeward cylinder at (a) $Re = 6.5\times10^4$ and (b) 9.7×10^3.

3.2 Strouhal numbers and spectral signatures

Fig. 4 illustrates spectral analysis results of the fluctuating lift at $Re = 6.5\times10^4$ and 9.7×10^3. Results at $Re = 3.2\times10^4$ and 1.6×10^4 were similar to $Re = 6.5\times10^4$ and 9.7×10^3, respectively, hence not presented. At $Re = 6.5\times10^4$, three St are seen for $L^* \le 1.5$ (Fig. 4a). The first St which is smaller than St_0 is connected to the vortex shedding, while the second and third St are second and third super-harmonics of the first one. Reattaching onto front-side surface of the leeward cylinder, the windward cylinder shear layer flows in the upstream direction and reattaches behind the windward cylinder forming a recirculation region between the cylinders (Fig. 2a). The entrainment from the recirculation to the shear layer weakens the shear layer velocity, resulting in a smaller St connected to the vortex shedding. The flow structures (Fig. 2a) explains why the second and third super-harmonic St exist in this L^* range.

At $1.5 < L^* < 2.2$ where only one peak is seen, the shear layer reattaching on the front-side surface goes on the same side to the downstream (Fig. 2b). On the other hand, the shear layer reattaching on front surface dives on the other side for $2.2 \le L^* \le 2.7$ (Fig. 2c) and the leeward cylinder generates a shear layer (dashed line). Therefore three shear layers interact around the leeward cylinder, producing the third superharmonic peak in the power spectra (Fig. 4a). It is interesting that when the wind cylinder shear layer after reattaching on the leeward cylinder goes into the gap between the cylinders (Figs. 2a, c), second and/or third superharmonic St appear (Fig. 4). With further increases in L^*, the shear layer again reattaches on the front-side surface and passes on the same side (Fig. 2d), which results in a single peak at $2.7 < L^* \le 3.9$ (Fig. 4a). The bistable flow occurs at $L^* = 4.0$ ($3.9 < L^* < 4.2$) corresponding to two peaks (Fig. 2e, 4a), followed by a co-shedding flow at $L^* \ge 4.2$ with a single peak (Fig. 2f, 4a). The $L^* = 4.0$ is called as the critical spacing.

At $Re = 9.7\times10^3$, St drops drastically from 0.259 to 0.215 between $L^* = 1.1$ and 1.3 (Fig. 4b). The drop is connected to a change in flow structure from an over-shoot flow (Fig. 2g) to a rear-side reattachment flow (Fig. 2h). The rear-side reattachment flow takes place at $1.3 \le L^* < 1.7$ where St is higher than St_0 and decreases slightly due to a forward advancement of the reattachment point. Further increase in L^* leads to a front-side reattachment flow for $1.7 \le L^* \le 3.5$ (Fig. 2i) where St drops from 0.191 to 0.146. The front-side reattachment flow corresponds to a St smaller than St_0. St is about 0.19 for $L^* \ge 3.9$, insinuating a co-shedding flow (Fig. 2k). Two peaks with different St values are seen at $L^* = 3.7$, indicating a bi-stable flow between the front-reattachment and co-shedding flows (Fig. 2j).

3.3 Flow structure map

C_{Df} and C_{Lf}, and St all are connected to flow structures. A flow structure map can therefore be drawn from the discussion made above and contour plots of C_{Df} and C_{Lf}, and St shown in Figs. 5, 6 and 7, respectively. A detailed flow structure map is displayed in Fig. 8. Transition in the shear layer being crucial parameter plays a role in the modification of flow structure and hence of forces and St. For a single cylinder in a free-stream, the transition length measured from the center of the cylinder decreases rapidly from $1.4D$ to $0.2D$ when Re increases from 2.0×10^3 to 6.5×10^4 [1]. This explains why the over-shot flow or rear-side reattachment flow occurs at the low Re ($= 9.7\times10^3$) but not at the higher Re ($= 6.5\times10^4$, Fig. 2). It has been shown that St is highly dependent on Re for $L^* < 2$ but not so much for $L^* > 2$. This is due to the fact that the windward cylinder shear layer transition happens around the leeward cylinder for $L^* < 2$. It shifts to the upstream with Re, so does the reattachment position. On the contrary, it occurs much upstream of the leeward cylinder for $L^* > 2$. C_{Df} and C_{Lf} vary significantly with Re even for the $L^* > 2$. Reattachment position and incidence angle of the shear layer on the cylinder are responsible for this variation. Since transition happens between the cylinders, reattachment position and angle of incidence on the cylinder vary significantly with Re.

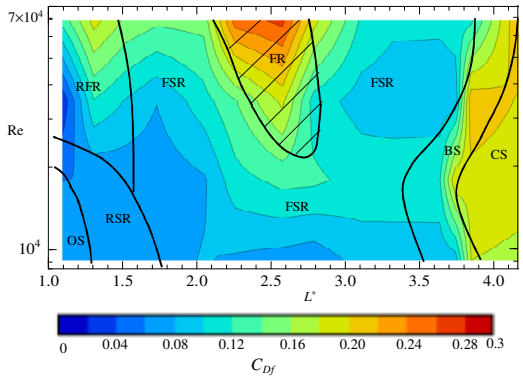

Fig. 5 Contours of fluctuating lift coefficient C_{Df} on Re - L^* plane and flow structure map. OS: Over-shoot flow; RSR: rear-side reattachment flow; FSR: front-side reattachment flow; FR: front reattachment flow; RFR: reverse-flow reattachment flow; BS: bi-stable; CS: co-shedding.

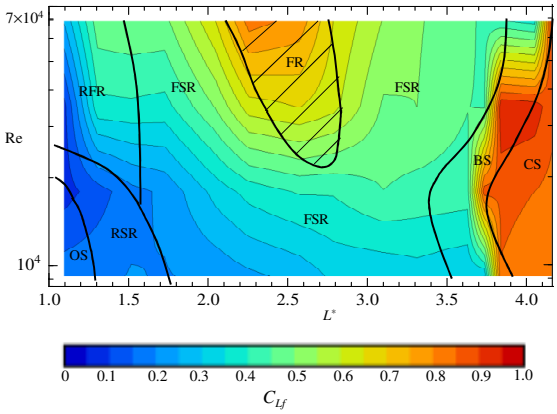

Fig. 6 Contours of fluctuating lift coefficient C_{Lf} on Re - L^* plane and flow structure map.

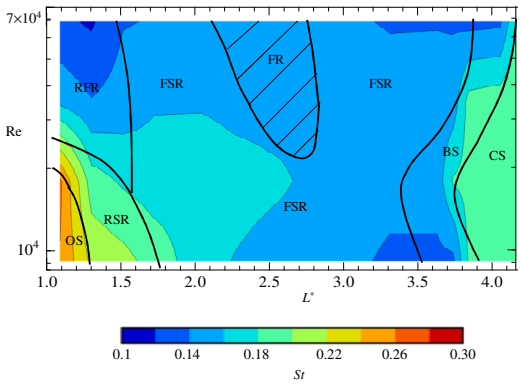

Fig. 7 Contours of Strouhal number *St* on *Re* - L^* plane.

How the flow structure changes with Re is dependent on L^* and can be explicated now. At small L^* (< 1.3), transition in the windward-cylinder shear layer occurs behind the leeward cylinder for smaller Re (<1.8×10^4), thus an over-shoot flow (OS) is possible. When Re is increased to about 2×10^4, the transition shifting upstream causes the shear layer to bow more and hence to reattach on the rear-side surface of the leeward cylinder (RSR). Further increase in Re (> 2×10^4) is accompanied by a further shift in the transition and a further bow in the shear layer. The shear layer therefore reattaches on the front-side surface, which results in a strong reverse flow reattaching on the rear surface of the windward cylinder (RFR). When L^* is increased to 1.3 ~ 1.75, the shear layer reattaches on the rear-side surface at Re < ≈1.7×10^4 (RSR). An increase in Re causes the shear layer to reattach on the front-side surface with the reverse flow reattachment (RFR, L^* < 1.6) and without the reverse flow reattachment (FSR, L^* > 1.6). At L^* = 1.75 ~ 3.5, the shear layer reattaches on the front-side surface (FSR) at Re < 2×10^4. It is interesting that when Re is increased (Re > 2×10^4), shear layer reattachment occurs on the front surface (FR) at an island like region (L^* = 1.8~2.8) marked by the hatched lines. Indeed, the 'kink' in C_D distribution and peak in C_{Df} and C_{Lf} distributions appear in this region. With further augments in L^*, bistable flow (BS) appears at L^* =3.4 ~ 4.1 depending on Re, followed by co-shedding flow.

4. Conclusions

Our findings reveal that C_{Df}, C_{Lf} and St are strong functions of Re and L^*. St diminishes, and C_{Df} and C_{Lf} augment with increasing Re. C_{Df}, C_{Lf} and spectral patterns are qualitatively similar at Re = 9.7×10^3 and 1.6×10^4, but different from those at Re = 3.2×10^4 and 6.5×10^4. With increasing L^* from 1.1 to 4.5, flow structure at Re = 9.7×10^3 changes as over-shoot (L^* < 1.3), rear-side reattachment ($1.3 \le L^* < 1.7$), front-side reattachment ($1.7 \le L^* \le 3.5$), bi-stable ($3.5 < L^* < 3.9$) and co-shedding ($L^* \ge 3.9$), while that at Re = 6.5×10^4 changes as reverse-flow reattachment ($L^* \le 1.5$), front-side reattachment ($1.5 < L^* < 2.2$), front reattachment ($2.2 \le L^* \le 2.7$), front-side reattachment ($2.7 < L^* \le 3.9$), bi-stable ($3.9 < L^* < 4.2$), and co-shedding ($L^* \ge 4.2$). The major difference in the flow structures between the two Re is that the over-shot flow and rear-side

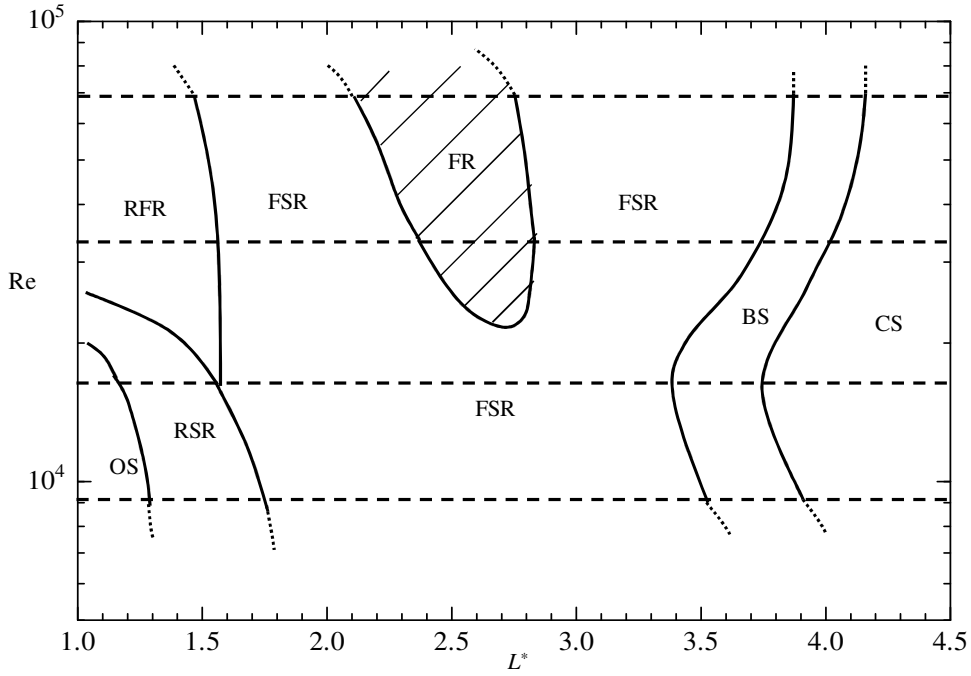

Fig. 8 Flow structure map with variation in *Re* and L^*. The hatched is the region where the kink in C_D distribution and peak in C_{Df} and C_{Lf} distributions occur. While the horizontal dashed lines represent the Re examined, the dotted lines are the predicted/extended boundaries.

reattachment flow prevail at Re = 9.7×10^3 - 1.6×10^4 and the reverse-flow reattachment flow and front reattachment flow appear only at Re = 3.2×10^4 - 6.5×10^4. Transition in the shear layer plays a major role behind the difference. The 'kink' in C_D distribution obtained in the literature or peak in C_{Df} and C_{Lf} for Re = 3.2×10^4 - 6.5×10^4 is connected to front reattachment flow (FR) where the windward cylinder shear layer reattaching on the front surface of the leeward cylinder sweeps to the other side of the cylinder.

5. Acknowledgments

Alam wishes to acknowledge supports given to him from the Research Grant Council of Shenzhen Government through grants JCYJ20120613145300404 and JCYJ20130402100505796. The author is also grateful to Professor Hiroshi Sakamoto, Kitami Institute of Technology, for his support to conduct this experiment in his laboratory.

REFERENCES

[1] M.M. Zdravkovich, Review of flow interference between two circular cylinders in various arrangements, *Journal of Fluids Engineering*, *Trans. of ASME,* Vol. 99, pp 618–633 (1977).

[2] M.M. Alam, J.P. Meyer, Global aerodynamic instability of twin cylinders in cross flow, *Journal of Fluids and Structures*, Vol. 41, pp 135-145 (2013).

[3] D. Sumner, Two circular cylinders in cross-flow: a review, *Journal of Fluids and Structures,* Vol. 26, pp 849–899 (2010).

[4] D. Biermann, Jr. Herrnstein, The interference between struts in various combinations, *National Advisory committee for Aeronautics*, Tech. Rep. 468 (1933).

[5] M.M. Zdravkovich, D.L. Pridden, Interference Between Two Circular Cylinders; Series of Unexpected Discontinuities, *Journal of Industrial Aerodynamics*, Vol. 2, pp 255-270 (1977).

[6] M.M. Alam, M., Moriya, K. Takai, H. Sakamoto, Fluctuating fluid forces acting on two circular cylinders in a tandem arrangement at a subcritical Reynolds number, *Journal of Wind Engineering and Industrial Aerodynamics*, Vol. 91, pp 139–154 (2003).

[7] T. Igarashi, Characteristics of the flow around two circular cylinders arranged in tandem (2nd Report), *Bull. of the Japan Society of Mechanical Engineers*, Vol. 27, pp 2380–2387 (1984).

[8] G.V. Papaioannou, D.K.P. Yue, M.S. Triantafyllou, G.E. Karniadakis, On the effect of spacing on the vortex-induced vibrations of two tandem cylinders, *Journal of Fluids and Structures*, Vol. 24, pp 833–854 (2008).

[9] M.M. Alam, H. Sakamoto, Y. Zhou, Determination of flow configurations and fluid forces acting on two staggered circular cylinders of equal diameter in cross-flow, *Journal of Fluids and Structures*, Vol. 21, pp 363-394 (2005).

ICMIEE-PI-Keynote

Status of Natural Fiber Composites in Bangladesh and Their Potential Applications

Mubarak A Khan[1*], Jahangir A Khan[1,2] and Jahid M M Islam[1]

[1]*Institute of Radiation and Polymer Technology, Bangladesh Atomic Energy Commission, Dhaka-1000, Bangladesh*

[2]*Department of Chemistry, Narsingdi Govt. College, Narsingdi, Bangladesh*

ABSTRACT

Composite materials which are cost-effective, environmentally friendly, light-weight and also durable are being considered for diversified applications, such as furniture, building materials, automotive industry and many more. In the recent years, the natural fiber based composites are coming forward to solve the problem associated with the synthetic fiber based composites like non-biodegradability, CO_2 production during manufacture etc. The main research of natural fiber-reinforced polymer composites is to provide a suitable compatibilizer or coupling agent between the reinforcement and the polymer matrices because the polar nature of natural fibers makes them incompatible with non-polar polymer matrices. In this paper, the present status of the natural fiber based composite materials; especially jute fiber based composites have been discussed from diversified applications and promotional view because jute fiber is the most abundantly natural fiber in Bangladesh which has high cellulose content and a low micro-fibrillar angle. Composite materials with jute fabrics have been made successfully using radiation processing technology and chemical modifications for general purpose constructions like low cost housing, sanitary accessories etc. The sample showed 147MPa tensile strength, 150MPa bending strength, 68 kJm^{-2} impact strength and more than 50 years durability. The treatments provided a synergistic effect on the mechanical performances and facilitated to develop a strong, lightweight and durable infrastructural material with an affordable cost. Many value added products like corrugated sheet, roof tiles, room insulator, shading, kitchen fittings etc. were also prepared using the same technology. Many of the products were successfully delivered to the end users where very positive feedbacks were found. The eye catching successes of field trials have caught attention of several entrepreneurs who are very interested to commercialize the products. So, this jute based composite is very promising as an alternative of commonly used construction materials in rural and urban areas of Bangladesh as well as for preparing value added products for household purposes.

Keywords: Natural fiber, Jute, Composite material, Biodegradability

*Corresponding author: Email-makhan.inst@gmail.com

1. INTRODUCTION

Jute has high cellulose content and low micro-fibril angle which are desirable properties of a fiber to be used as reinforcement in polymer matrices. Jute is one of the most common natural fibers having high tensile modulus and low elongation at break. If the low density (1.45 g/cm^3) of this fiber is taken into consideration, then its specific stiffness and strength are comparable to respective quantities of glass fiber [1, 2, 3]. In spite of these above-mentioned advantages, jute fiber – like other natural fibers – exerts some difficulties while used as reinforcement in non-polar polymer matrices. Being polar and hydrophilic in nature, jute fiber exhibits poor interfacial adhesion with hydrophobic polymer matrices. To overcome these kinds of bottlenecks, many attempts, such as physical and chemical treatments, lead to changes in the surface structure and surface energy of the fibers.Such an effort was made to prepare a composite with improved mechanical properties using radiation induced jute-urethane polymer system. The resin matrix was prepared under gamma radiation using urethane acrylate in the presence of N-vinylpyrrolidone, ethyl hexyl acrylate and trymethylol propane triacrylate. Some additives such as acetic acid, acrylamide, urea, talc, and titanium oxide were incorporated into the formulation [4]. In this context, hessian cloth (jute product) was coated with urethane pre-polymer with different formulations in the presence of plasticizers under UV radiation. Tensile properties of the composites were found to increase. It is also indicative that simulated weathering and soil degradation tests show the biodegradable nature of the prepared composites [5]. A good correlation was found between composite impact damping and yarn toughness for the jute-epoxy composites [6]. Two monomers such as 2-

* Corresponding author. Tel.: +88-01819252292

E-mail address: makhan.inst@gmail.com

hydroxy ethyl methyl acrylate (HEMA) and 2-ethyl hexyl acrylate (EHA) were successfully used as novel coupling agents for jute fabric (hessian cloth) polypropylene composite. The mechanical properties of the resulting composites increased as a result of surface treatment of the jute fabrics [7]. Polyester resin was used as matrix material for composite fabrication. The mechanical properties (tensile and bending strengths) of the surface modified jute fabrics reinforced polyester composites improved significantly [8]. The unsaturated polyester resin is quite useful for industrial and civilian world. As a low-cost, rigid, high strength-to-weight material, one can find its products in the form of mechanical parts, pipes, tanks, electronic gears, etc.They can be cured to give insoluble, infusible solid plastics through a free radical curing process. Organic peroxides are employed as free radical initiators while tertiary aromatic amines and some organic metal salts, such as cobalt naphthenate, are used as curing promoters if needed Tertiary aromatic amine and cobalt naphthenate can significantly reduce the decomposition temperature of peroxides via chemical reduction processes [9]. The objective of this research work is to prepare low cost light weight, durable, earthquake and cyclone tolerance housing materials and so on likewise products with sustainable local technology.

2. MATERIALS AND METHODS

2.1. Materials

Jute fabric was used as the reinforcing agent. The matrix polymer was a commercial unsaturated polyester resin (EPOLAC G-153ALX) containing 1.5% cobalt napthenate solution, 6% cobalt catalyst as promoter, and 36% styrene as diluent. Methyl ethyl ketone peroxide (MEKP) and wax were used as curing agent and mold releasing agent respectively. REOLOSIL fumed silica (aerosealpowder)was used as filler. A substituted aromatic tertiary amine was used as coupling agent.

2.2. Methods

2.2.1. Surface Modification

Hessian cloth was cut into rectangles (12 ×10 cm^2) and temporarily fixed in a long square sized plate (50 ×50 cm^2) where UV radiation could be given together to six equal sized rectangular samples. Then the samples were subjected to UV radiation (254–133 nm) using an irradiator (UV minicure Me-200, ISTTechnik, Germany), which delivers apower strength of 2 kW. The speed of the manicure was 4 meter/minute for each pass of the substrate under the lamp by maintaining different UV radiation intensities expressed by number of passes.

2.2.2. Composite Fabrication

Composites were fabricated using a simple hand lay-up technique. The working surfaces were treated with releasing waxes to facilitate easy removal of samples from the mold surfaces. Cobalt napthenate(catalyst) and MEKP (curing agent) were mixed thoroughly with USP at various formulations before each operation. At the beginning of fabrication, a gel coat with 2% MEKP was uniformly brushed into the finished side of the male and female parts of the mold. After 1h, when curing of gel coat was completed, each layer of the fiber was pre-impregnated with formulations made of USP. The impregnated jute samples were then placed one over another as a sandwich. This sandwich was placed into a mould. Both parts of the mold were tightened by screw-bolt and allowed 3 h for total curing (composite fabrication). The composites were cut into rectangular pieces of equal size (120×100×3mm^3) for different tests. All results are taken as the average of five samples for each testing.

2.2.3. Mechanical Tests

The tensile and bending strength of the composites were measured according to DIN 53455 and DIN 53452 standard methods by a universal testing machine (Hounsfield S Testing Series, UK) with an initial clamp separation of 20 mm and a cross-head speed of 10 mm/min. Charpy impact strength of the composite was determined by an impact tester (MT-3016) according to the DIN EN ISO 179 standard in the flat wise, unnotched mode. The test samples were conditioned at 25°C and 50% relativehumidity for several days before testing and all the tests were performed under the same conditions.The result of each test is taken as the average value of five samples

3. RESULTS AND DISCUSSION

The effect of jute content (%wt) on the mechanical properties of the resulting composites is studied here and shown in Figures 1 and 2. It was found shows poor mechanical properties due to poor fiber population and low load transfer capacity to one another. levels of fiber content (such as 20%), the composite As a result, stress gets accumulated atcertain points of the composites and highly localized strains occur in the matrix. At intermediate levels of loading (30%), the population of the fibers is just right for maximum orientation and the fibers actively participate in stress transfer. So, the mechanical properties of the composite reaches maximum. At high levels (suchas 40%) of jute content, the non homogeneous fiber matrix adhesion becomes prominent which leads to agglomeration among the fibers and stress transfer gets blocked [10]. As a result, the mechanical properties of the composite again decreased. The composite of the optimized jute content (30%w/w) showed 205% increase in tensile strength (TS), 141% in tensile modulus (TM), 226% in bending strength (BS) and 195% in bending modulus (BM) than that of the resin based composite.

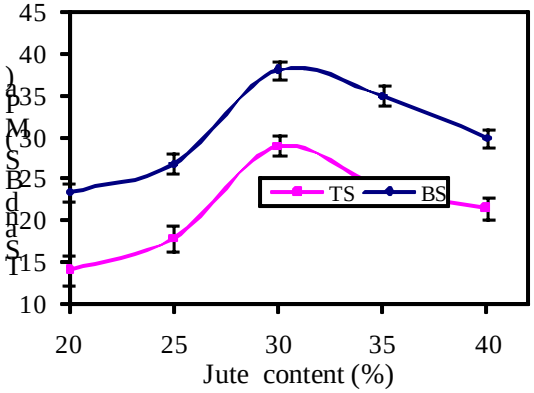

Figure 1: Effect of jute content on tensile and bending strength of composite

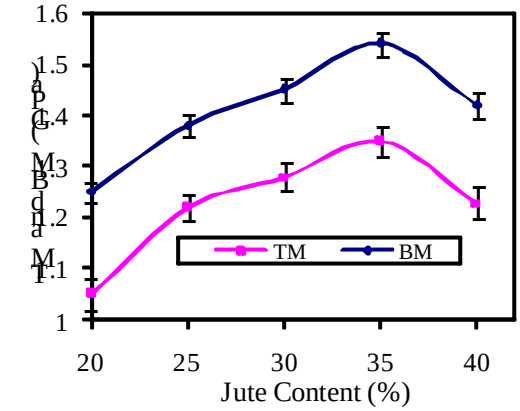

Figure 2: Effect of jute content on tensile and bending modulus of composites

The effect of UV radiation on the mechanical properties of jute based composites was investigated and presented in Figures 3 and 4. Jute content in the UV treated composite is maintained at about 30%. The UV intensities of different passes (200-400 pass) were exposed to jute surfaces.1 UV pass indicates 1 metre of UV exposure in the machine. It was found that UV intensity of 200 pass showed the highest mechanical properties. Mechanical properties, such as tensile and bending properties increase up to 200 pass, which gives 68% increase in TS, 78% in TM, 58% in BS, and 57% in BM relative to untreated jute-based composites. The TS, BS, TM and BM of the control composite were found 29.45 MPa, 38.35 MPa, 1.35 GPa and 2.54 GPa respectively. The increase of mechanical properties of the composite with increasing UV radiation may be due to the intercross-linking between the neighboring cellulose molecules, which results in the strength of jute fabrics. It is observed from Figures 3 and 4 that mechanical properties of the composite increase with UV pretreatment up to a certain limit and then decrease due to the two opposing phenomena, namely, photo cross-linking and photo degradation that take place simultaneously under UV radiation. At lower doses, free radicals are stabilized by a combination reaction and, as a result, photo cross-linking occurs. The higher the number of active sites generated on the polymeric substrate, the greater the grafting efficiency. But at higher radiation, the main chain may be broken-down and polymer may degrade into fragments and, as a result, mechanical properties were found to decrease after certain UV doses. An intense radiation results in a loss of strengths and a reduced degree of polymerization is observed [10].

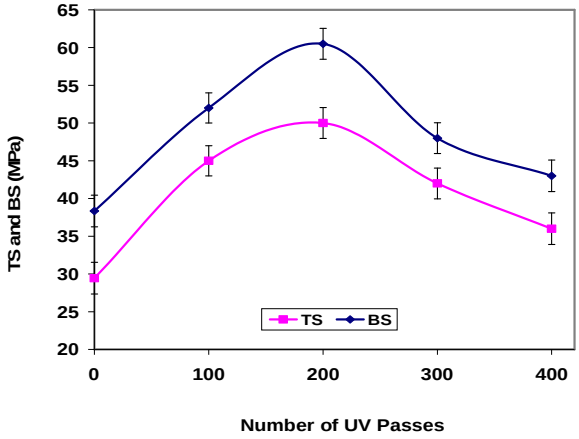

Figure 3: Effect of UV radiation on tensile and bending strength of jute-based composites

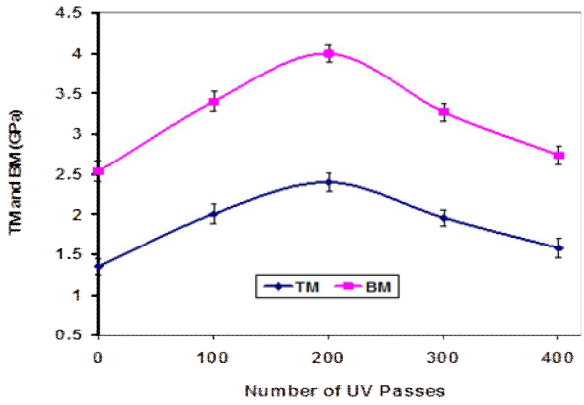

Figure 4: Effect of UV radiation on tensile and bending modulus of jute-based composites

Jute fabrics were further treated with a coupling agent (0.1 to 2.0 %) at the stage of pre-impregnating the fibers with USP resin to show its effect on to the composites. Figs 5 and 6 show the effect of coupling agent on the properties of the composites. The coupling agent with a concentration of 1.0 % performed the best of mechanical properties. It is also indicative that coupling agent treated composite showed much better mechanical properties than that of the control composite. It was found that 1.0% coupling agent treated composite showed 90, 74.7, 77.77 and 57.48% higher TS, BS, TM and BM values than that of the control composite.

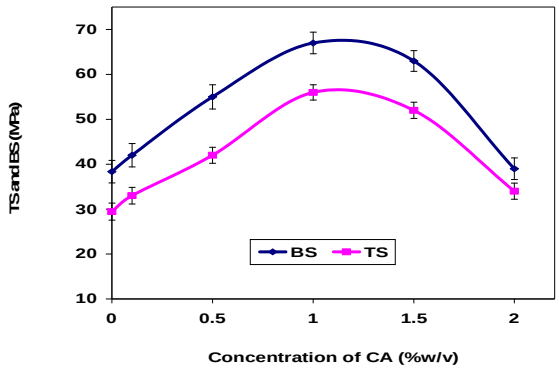

Figure 5: Effect of coupling agent on tensile and bending strength of composites

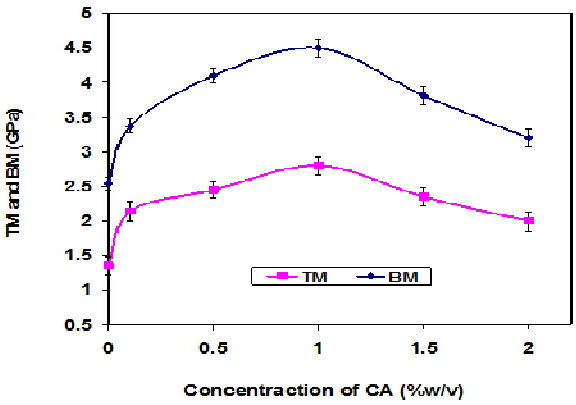

Figure 6: Effect of coupling agent on tensile and bending modulus of composites

4. Aging properties of Composite (JUTIN)

4.1. Thermal aging

Table 2.The effect of thermal aging on tensile strength of JUTIN

Sample	Room temp.	Tensile strength (MPa) 15 days			
		OºC	4ºC	50ºC	70ºC
Jutin	96	116±2.0	99.8±1.9	93±1.82	78±1.8

The JUTIN was subjected to undergo different temperature treatments at 15 days time periods to investigate the effect of thermal aging on tensile strength of JUTIN. It was found that the strength of composite increases with the decrease of temperature. The TS decreased to about 19.0 % and 3.0 % at aging temperature of 70ºC and 50ºC respectively. Whereas, in case of 4ºC and 0ºC, TS increased about 4.0% and 21.0% respectively.

4.2. Water aging

There is very negligible amount of water uptake (<1%) within 3 months. There is no change in mechanical properties within 3 months.

4.3. Normal weathering aging

The mechanical properties increased up to 7-10% within 6 months and remain unchanged up to 12 months.

5.4. Accelerated weathering aging

To study the weathering effect on the mechanical properties of Jutin, the samples of jutin were exposed under simulated weathering tester from Q-panel Co. (model QUV, USA). The weathering testing was performed in alternating cycles of sunshine over 4h (65º±2ºC) and condensation for 2h (45º±2ºC). This aging test was carried out for 600 h.Owing to this test the losses of mechanical properties more or less zero up to 300 hours and about 10% up to 600 h.

5. CONCLUSION

The tensile strength of the prepared composites composite is 150 MPa, bending strength is 147 MPa and impact strength is 68 kJm^{-2} and It will be stable up to 50 years. This jute-based polymer composite shows extra-ordinary features which are very promising to make jute based polymer composite as a effective alternative of metallic or plastic materials. It is rust proof, saline resistant, lightweight, heat resistant, sound proof, environmental friendly, Very low thermal expansion, and damaged area can be sealed very easily. In contrast, lightweight jute made composite boards fixed on steel frames with bolts & nuts are more flexible allowing lateral movements of the structures. They absorb and reduce seismic energy. The usage of natural fiber (jute) based products in post disaster management of rehabilitation & rebuilding, would become cost competitive compared to other building materials. Thus, all the properties of composite claim its position as an ideal building material.

REFERENCES

[1] Soumitra Biswas, Atul Mittal & G Srikanth, Gujarat Earthquake - Composite Materials towards Re-building & Rehabilitation

[2] Bogoeva-Gaceva G., Avella M., Malinconico M., Buzarovska A., Grozdanov A., Gentile G. and Errico M.E. (2007). Natural fiber eco-composites.*Polymer Composite*;28: 98-107.

[3] Joshi S.V., Drzal L.T., MohantyA.K.andArora S. (2004). Are natural fiber composites environmentally superior to glass fiber reinforced composites? *Composites:Part A*; 35: 371-376.

[4] Khan M.A., Ali K.M. I., Balo S.K. and Ahmad, M.U. (1998). Effect of additives reinforcement of radiation induced jute urethane polymer composites. *Journal of Applied Polymer Science*; 67:79-85.

[5] Khan M.A., Uddin M.K. and Ali K.M.I. (1997). Degradable jute plastic composite.*Polymer Degradation and Stability*; 55:1-7.

[6] Gassan J. and Bledzki A. K. (1999). Possibilities for improving the mechanical properties of jute/epoxy composites by alkali treatment of fibers.*Composites Science and Technology*; 59:1303-1309.

[7] Khan M.A., Hinrichsen G. and Drzal L.T. (2001). Influence of novel coupling agents on mechanical properties of jute reinforced polypropylene composites. *Journal of Materials Science Letters*; 20:1711-1713.

[8] Mohanty A.K, Khan M.A. and Hinrichsen G. (2000). Influence of chemical surface modification on the properties of biodegradable jute fabrics-polyester amide composites. *Composites:Part A*; 31:143-150.

[9] Khan M.A., Ganster J. and Fink H. P. (2004). Natural and man-made cellulose fiber reinforced hybrid polypropylene composites.5th Global Wood and Natural Fiber Composites symposium, in Kassel, Germany, April 27-28.

[10] KuangW. and Richardson, A. (2007).A New Amine Promoter for Low-temperature Cure of MEKP Initiated Unsaturated Polyester Resin Systems. *Composites Research Journal;* 1(4): 9-13.

[11] Abdullah-Al-Kafi, Abedin M. Z, Beg M. D. H, Pickering K. L and Khan M. A (2006). Study on the Mechanical Properties of Jute/Glass Fiber-reinforced UnsaturatedRadiation Polyester Hybrid Composites: Effect of Surface Modification by Ultraviolet Radiation. *Journal of Reinforced Plastics and Composites*; 25: 575-588.

[12] Khan, M. A. and Hasan, M. M. (2004). Surface Modification of Natural Fibers by Photo-grafting and Photo-curing, In: Mital, K. L. (ed.), Polymer Surface Modification: Relevance to Adhesion, VSP, Vol. 3, pp. 263–283.